JTTEE5 19:723–735
DOI: 10.1007/s11666-010-9490-3
1059-9630/$19.00 © ASM International



# Sensor Issues and Requirements for Developing Real-Time Control for Plasma Spray Deposition

*D. Wroblewski, G. Reimann, M. Tuttle, D. Radgowski, M. Cannamela, S.N. Basu, and M. Gevelber*

*(Submitted August 7, 2009; in revised form February 9, 2010)*

**This paper discusses the requirements of sensors that could be used both for advanced real-time control as well as manual torch operator control of plasma spray processes, and reviews the critical issues associated with design and implementation of such sensors. The focus is on yttria-stabilized zirconia for thermal barrier coatings. The overarching requirement is that the sensor must capture the subset of particles that contributes most to coating properties and that the resulting measurements of these critical subdistributions must be aggregated in a manner that correlates best to the coating buildup. For deposition rate control, the focus of this work, experiments show that the mass flux of molten particles correlates better with coating thickness than bulk-average temperature or light intensity. However, measurement of molten mass flux for control requires sensors that are capable of sensing particle states at high rates from across a large portion of the full plume.**

**Keywords** ceramic oxide layers, coatings for gas turbine components, diagnostics and control

## 1. Introduction

The plasma spray process is characterized by a wide distribution of particle states as well as large variations of the process itself that introduce significant variations in both coating thickness and structure. These variations reduce yield, limit process optimization, increase cost, and lengthen development time for new parts and materials. To combat these variations, sensors have been developed to provide operators with the information they need to make a spray/no-spray decision and to adjust inputs to bring the process within specification.

To obtain a better understanding of the need for improved sensing and control technology, studies were conducted with a major plasma spray contract manufacturer to quantify the impact of process variation. Throughout actual production runs (over 400 h) utilizing a Sulzer-Metco 7 MB torch (nitrogen/hydrogen), flat substrates were sprayed with yttria-stabilized zirconia (YSZ) and the coating thickness and density (reflective of coating porosity) were measured. The density was measured by measuring the dimensions of the coating with calipers and its thickness with a micrometer; the mass was determined by before and after measurements on an analytical balance. The overall error in the density measurement is estimated to be 5%, while error in thickness measurement is about 1%. These results, shown in Fig. 1 and 2, reveal that not only are there large variations (±15% for a target thickness of 250 μm) in coating thickness and density (±10%), but also that these variations are not correlated with each other. The large standard deviation of coating thickness (0.08 relative to the normalized average thickness) implies that unless the specification window is large, significant re-work will be required. Each re-worked piece wastes booth time and powder, which increases production costs as compared to a well-controlled process with lower variation.

The objective of this paper is to address the issues and requirements for sensors that could be used to reduce the variations in deposition rates for plasma-sprayed parts. The operation of established sensing schemes is reviewed (Section 2), and issues associated with selectively measuring the molten particle ensemble are discussed (Section 5). A series of deposition experiments (Section 3) were carried out with three different torches, the SG-100 (internal injection), Sulzer 9 MB, and F4 (external injection), operated under a variety of conditions. Detailed analysis of these experiments as they relate to control of deposition rate (Section 6) constitute the empirical foundation for both the theoretical analysis of particle state distributions (Section 4) and specific requirements for deposition rate control sensors (Section 7).

## 2. Sensor Schemes

The most common sensors for plasma spray monitoring and control fall into two main categories: (1) fiber-optic based sensors that typically image a small measurement

**D. Wroblewski, M. Cannamela, S.N. Basu,** and **M. Gevelber**, Mechanical Engineering Department, Boston University, Boston, MA; and **G. Reimann, M. Tuttle,** and **D. Radgowski**, Cyber Materials LLC, Boston, MA. Contact e-mail: dew11@bu.edu.

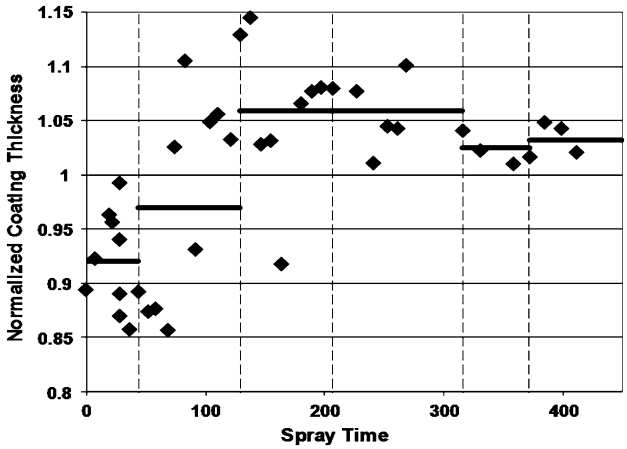


**Fig. 1** Normalized coating thickness variation observed in spraying of flat plate test substrates during production runs, showing large variation over 400 h. Each diamond is a measurement, *dotted vertical lines* are gun rebuilds, and *solid horizontal lines* are the average coating thickness between gun rebuilds. Measurement uncertainty is estimated at 1% (Ref 14)

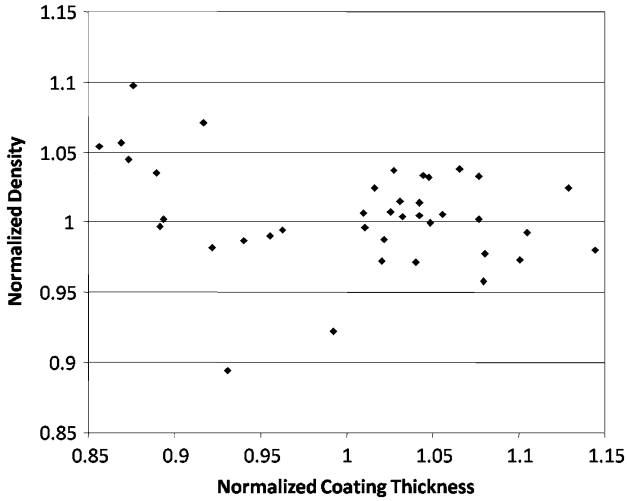


**Fig. 2** Density vs. coating thickness for test substrates sprayed during production runs. Measurement uncertainty estimated at 5% (Ref 14)

volume onto a pair of photo-detectors (either solid-state or photo-multiplier tubes) and detect either individual particles or ensembles of particles, and (2) CCD arrays (either 1D or 2D) that image the plume in a single line at a specific point along the spray direction, or both along the vertical and spray directions, providing bulk-average properties of the plume, individual particle states, or both.

Temperature measurements are based on multicolor pyrometry, which relates intensities in two or more wavelength bands to temperature based on Planck's blackbody radiation function. Most common sensors employ two-color pyrometry, for which the signal is split and filtered by two narrow band filters, with the ratio proportional to temperature. Compared to light intensity-based temperature measurements, the two-color approach eliminates the first order effect of emissivity, but does not account for differences in emissivity between the two wavelength bands—i.e., nongray body behavior (see Section 4.2). Multiwavelength measurements can be used to reduce the effects of nongray emission behavior. For example, by using three colors and an assumption of linear variation of emissivity with wavelength, both temperature and emissivity can be estimated (Ref 1).

### 2.1 Fiber-Optic Based Sensors

For single particle sensors, the detector provides a time-resolved measurement of individual particles, which appear as a pulse signal of light intensity versus time. Velocity is obtained from the lag time of the signal peak detected at two different axial positions, while peak values of light intensity are used for pyrometry. Particle diameter can be found assuming that peak light intensity is proportional to the surface area of the particle and temperature to the fourth power, resulting in

$$d = C\sqrt{I/T^4}, \qquad \text{(Eq 1)}$$

where $C$ is a calibration constant and $I$ is the peak light intensity.

The DPV 2000 (Tecnar, St. Bruno, QC, Canada) (Ref 2), the most popular single particle sensor, has a measurement volume smaller than 1 $mm^3$. Its two-color pyrometry is based on wavelength bands at 787 ± 25 and 995 ± 25 nm, chosen to minimize interference with scattered plasma radiation, which occurs at discrete lines. The Individual Particle Monitor (IPM, InFlight, Idaho Falls, ID) is another single particle sensor.

A bulk-averaged velocity and temperature can be obtained from a cross correlation of signals from the two positions over a time window that includes multiple peaks/particles. The Tecnar Accuraspray is an example of this type of sensor (Ref 3) based on the same concepts as the DPV-2000, but with a larger measurement volume. The Inflight Individual Particle Pyrometer (IPP), measures a bulk-average temperature over a pencil-sized volume that spans the lateral dimension of the plume.

### 2.2 CCD Arrays

CCD arrays (either linear or 2D) measure light intensity averaged over the pixels' integration time, which is typically longer than the particle resident time within the imaged field of view. The intensities detected in a single frame, obtained with a short exposure of a column in the array will reveal a series of pulses from the light intensity of particles that passed through the array's field of view. By knowing the size of the pixels in the array, particle diameter can be determined from these images directly, while the temperature can be determined by standard pyrometry and the velocity can be calculated from the total intensity measured. Large CCD arrays enable measurement of particle states from the whole plume height at once, dramatically increasing the speed for full-plume

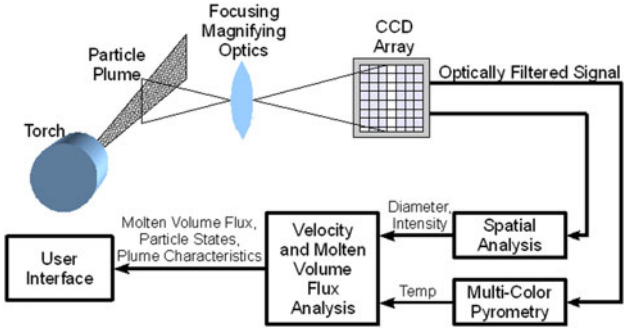


**Fig. 3** Schematic of the Flux Sentinel showing signal acquisition, data flows, and calculation steps

sensing versus individual particle sensors, which must scan to cover the entire plume.

The Flux Sentinel (Cyber Materials, Boston, MA) has developed such a CCD-based sensor capable of sensing individual particle temperature, diameter and velocity across the entire plume (see schematic in Fig. 3). An array column is used with a resolution of 3.5 μm to directly measure particle diameter and since the array is long enough, it can measure particles from across the whole plume. Particle diameter is estimated photometrically from the shape and extent of portions of the signal identified as particle images using topological criteria. Particle images are transformed by the transfer function of the intervening optics, and include additive noise from the instrument's electronics. Cyber Materials has developed filtration techniques to mitigate the impact of noise and optical aberrations, defocus being by far the most prominent, on the accuracy of diameter measurements. The combination of rejection of particle images failing quality criteria and enhancement of those images that pass has proven effective in this regard.

Multiple-color pyrometry is used to determine the temperature for each particle using 125 nm-wide color bands. Assuming gray-body emission from the particles, the map from temperature to intensity for each color band is found by integrating Planck's blackbody radiation function ($E_{B\lambda}$) for each temperature against the known spectral sensitivity of the sensor ($S_i$).

$$I_{Ci}(T) = \int_{\lambda_{1,i}}^{\lambda_{2,i}} S_i(\lambda) E_{B\lambda}(T,\lambda) d\lambda, \qquad \text{(Eq 2)}$$

where $I_{Ci}$ is the intensity in the $i$th color band. The temperature is then found using a least square fit of the relative values of measured intensity in the multiple bands compared to the calculated values from Eq 2.

Frames are sampled at 500 Hz and since the exposure time is longer than the particle's transit time across the measurement volume, multiple particles are captured in each frame. Particle velocity is calculated through the Boltzmann relation via the measured particle intensity, which is approximately proportional to the surface area of the particle and temperature to the fourth power, by:

$$v = \frac{CD^2T^4}{I}, \qquad \text{(Eq 3)}$$

where $T$ and $D$ are the measured temperature and diameter of a given particle and $I$ is the sum of intensity from all pixels in that particle's image. The constant $C$ subsumes the emissivity of the particle material as well as optical view factor, sensor efficiency, and analog to digital quantization factor. An analysis of measurement error and calibration procedure for the constant $C$ will be presented in a future paper.

Long integration times or averages of many frames from CCD arrays can provide a smooth light intensity curve that represents the sum of all particles imaged by the array; thus, the Flux Sentinel can also provide overall light intensity measurements, in addition to individual particle statistics. This provides an ability to measure the shape and location of all the particles in the plume. The Inflight Torch Diagnostic Sensor (TDS) is an example of this type of long integration time sensor and the Accuraspray includes such a CCD in their sensor package.

The time-averaged nature of a CCD array signal induces a velocity sensitivity, since for a given temperature, diameter, and integration time, faster particles will spend less time in and emit less light into the sensing volume. Though this effect can be used for indirect measurement of velocity, it also has implications for various sensing issues (see Section 4).

Two-dimensional arrays that image the entire plume can be used to measure velocity vector (speed and direction) directly through analysis of streaklines on the 2D image. They can also provide bulk-average temperatures, typically using long integration times, which lead to the same velocity sensitivity described above. The SprayWatch (Oseir Ltd., Tampere, Finland) is an example of this type of sensor (Ref 4).

## 3. Experiments

Most of the experimental results presented in this paper were obtained in the Advanced Materials Process Control Laboratory's plasma spray facility at Boston University (Ref 5). Experiments with the F4 torch were conducted at the Center for Thermal Spray Research at the University of New York in Stony Brook. Experiments were run with the SG100 torch (Praxair Surface Technologies, Indianapolis, IN) with internal injection and the 9 MB torch (Sulzer-Metco, Westbury, NY) with external injection. The torches are fed through a Model 1264 powder feeder (Praxair Surface Technologies, Indianapolis, IN) operated at a 3 rpm feedrate. Diagnostics include: a Tecnar DPV-2000 (DPV), Inflight Particle Pyrometer and Torch Diagnostic System (IPP/TDS), Inflight Individual Particle Monitor (IPM), and a Cyber Materials Flux Sentinel (FS). High-speed voltage and acoustic measurements are used to monitor torch wear,

**Table 1 Experimental Conditions**

| Condition # | Torch type | Current, A | Primary gas, slm | Secondary gas, slm | Carrier gas, slm | Feedrate, rpm | F.S. rate, Particle/s | DPV rate, Particles/s | Powder |
|---|---|---|---|---|---|---|---|---|---|
| 1 | F4 | 650 | 60.1 | 4.4 | 5 | ··· | 138 | 255 | HW153 |
| 2 | F4 | 550 | 47.5 | 6 | 4 | ··· | 427 | 199 | HW153 |
| 3 | F4 | 450 | 59.7 | 11.1 | ··· | ··· | 134 | 240 | HW153 |
| 4 | F4 | 450 | 35.2 | 2.6 | ··· | ··· | 406 | 244 | HW153 |
| 5 | F4 | 650 | 35.2 | 2.6 | 3.8 | ··· | 1068 | 217 | HW153 |
| 6 | F4 | 450 | 60.1 | 4.4 | 3.5 | ··· | 32 | 265 | HW153 |
| 7 | F4 | 650 | 35 | 6.5 | 3.5 | ··· | 1584 | 171 | HW153 |
| 8 | SG100 | 600 | 40 | 10 | 5 | 3 | 1210 | | 10-75 μm |
| 9 | SG100 | 700 | 40 | 10 | 5 | 3 | 1852 | | 10-75 μm |
| 10 | SG100 | 800 | 40 | 10 | 5 | 3 | 2478 | | 10-75 μm |
| 11 | SG100 | 700 | 48 | 12 | 5 | 3 | 1492 | | 10-75 μm |
| 12 | SG100 | 700 | 32 | 8 | 5 | 3 | 1932 | | 10-75 μm |
| 13 | SG100 | 600 | 48 | 12 | 5 | 3 | 983 | | 10-75 μm |
| 14 | SG100 | 800 | 32 | 8 | 5 | 3 | 2618 | | 10-75 μm |
| 15 | SG100 | 700 | 40 | 10 | 2.5 | 3 | 1574 | | 10-75 μm |
| 16 | SG100 | 700 | 40 | 10 | 3.5 | 3 | 2096 | | 10-75 μm |
| 17 | SG100 | 700 | 40 | 10 | 4.5 | 3 | 1873 | | 10-75 μm |
| 18 | SG100 | 700 | 40 | 10 | 5.5 | 3 | 1625 | | 10-75 μm |
| 19 | SG100 | 700 | 40 | 10 | 6.5 | 3 | 1252 | | 10-75 μm |
| 20 | 9 MB | 600 | 40 | 6 | 5.5 | 3 | 638 | 124 | 45-75 μm |
| 21 | 9 MB | 600 | 40 | 6 | 6 | 3 | 483 | 194 | 45-75 μm |
| 22 | 9 MB | 600 | 40 | 6 | 6.5 | 3 | 574 | 195 | 45-75 μm |
| 23 | 9 MB | 600 | 40 | 6 | 7 | 3 | 315 | 191 | 45-75 μm |
| 24 | 9 MB | 600 | 40 | 6 | 7.5 | 3 | 330 | 190 | 45-75 μm |
| 25 | 9 MB | 550 | 40 | 6 | 6.5 | 3 | 333 | 207 | 45-75 μm |
| 26 | 9 MB | 500 | 40 | 6 | 6.5 | 3 | 489 | 214 | 45-75 μm |
| 27 | 9 MB | 600 | 43.3 | 6.5 | 6.5 | 3 | 226 | 220 | 45-75 μm |
| 28 | 9 MB | 600 | 36.7 | 5.5 | 6.5 | 3 | 318 | 196 | 45-75 μm |
| 29 | 9 MB | 500 | 40 | 6 | 5.5 | 3 | 236 | | 45-75 μm |
| 30 | 9 MB | 525 | 40 | 6 | 5.5 | 3 | 363 | | 45-75 μm |
| 31 | 9 MB | 525 | 40 | 6 | 5.5 | 3 | 331 | | 45-75 μm |
| 32 | 9 MB | 550 | 40 | 6 | 5.5 | 3 | 369 | | 45-75 μm |
| 33 | 9 MB | 575 | 40 | 6 | 5.5 | 3 | 424 | | 45-75 μm |
| 34 | 9 MB | 600 | 40 | 6 | 5.5 | 3 | 426 | | 45-75 μm |
| 35 | 9 MB | 600 | 40 | 6 | 6.5 | 3 | | 153 | 45-75 μm |

10-75 powder is Saint Gobain #204 and 45-75 is Saint Gobain #204b

and a linear CCD camera provides real-time light intensity distributions that can be used for closed loop control of spray pattern position.

The operating conditions used for the experiments are shown in Table 1. The majority of the data reported here was obtained with the DPV-2000 or the Flux Sentinel. As conditions are changed, the DPV-2000 was repositioned along the direction lateral to the injection direction and along the plume height using the auto-centering feature; however, the DPV operation manual does not explicitly state how this center is defined (e.g., particle number flux, interpolated maximum, light intensity maximum, etc.). The number of particles sensed for each experiment is shown in Table 1. Note that the Sentinel is collecting particles across the entire plume while the DPV is collecting data at a single location.

Samples 1-19 were $25 \times 100$ mm$^2$ stainless steel coupons, and samples 20-34 were $25 \times 100$ mm$^2$ mild steel coupons. Each sample was sprayed with 15 layers proceeding from right to left in steps of 5 mm, at a torch velocity of 100 mm/s. Three different spray protocols were followed: for conditions 1-7, the entire substrate was sprayed; for conditions 8-19, only the center portion of the substrate was sprayed; and for conditions 20-34, the substrate was sprayed through a 0.75 in. diameter circular mask positioned over the center of the sample. Plume measurements were taken before the spraying. For conditions 20-28, for which multiple sensors were used, the plume was observed by first the DPV, then the IPP, and finally the Flux Sentinel. The mass of the coating was determined from before and after measurements of the sample's mass. All reported data were subsequently derived from these measurements.

## 4. The Nature of Particle State Distribution

Molten particles are the dominant contributor to the buildup of the deposited coating; hence, we focus on the distribution of this subset of particles in our measurement and sensing efforts. The dynamics of molten particle impingement and solidification are determined by the particle size, temperature, velocity, and flux rate of these molten particles. These particle metrics must therefore be the basis of any process measurement system that predicts coating qualities. However, developing a measure of these

particles is difficult due to the wide distribution of particle states in the plasma plume. These distributions are rooted in complex physics associated with the thermal, fluid, and electrical interactions between particle and plasma, and in the inherent nonuniformities associated with these interactions. Specifically, the source of distributions include the large gradients in the plasma jet, the intrinsic unsteadiness of the plasma jet, the stochastic nature of the injection process, and the prior distribution of particle diameters, all of which affect the particle trajectories and hence their thermal and momentum histories.

### 4.1 Molten Volume Ensemble

There are two critical aspects of the particle state distributions that impact measurement requirements for control systems. First, only a subset of the particles in the plume become incorporated in the coating—primarily those that are molten. The characteristics of this molten volume ensemble (MVE) differ from those of the entire ensemble, with the MVE characterized by smaller, hotter, and faster particles (Ref 6). For example, the diameter effects are shown in the distributions in Fig. 4(a) and (b) obtained with the Flux Sentinel at conditions 4 and 7 in Table 1, respectively. Effective control of coating thickness and other properties requires the ability to measure the particle states of this critical subdistribution in large enough numbers in order to provide a sensor signal suitable for control. For the analysis presented in this paper of both DPV and FS measurements, molten particles were taken as those particles measured to have a temperature above the reported melting temperature for that material.

Second, of the particles that end up in the coating, one must consider which particles contribute the most to the deposited coating. Thus, any metric used for control should be volume-weighted to properly reflect the particle's contribution to the coating. For example, the total molten volume flux is a properly weighted metric that has been shown to correlate well with deposited mass (Section 6),

$$\mathrm{MVF} = \frac{1}{t_\mathrm{M}} \sum_{i=1}^{N_\mathrm{MVE}} \frac{4}{3}\pi (D_i/2)^3, \qquad \text{(Eq 4)}$$

where $N_\mathrm{MVE}$ is the number of particles in the MVE, and $t_\mathrm{M}$ is the time over which the particles are captured by the sensor.

In general, volume-weighting would eliminate the bias toward smaller particles inherent with straight number averages, as illustrated in the number and volume-weighted temperature (Fig. 5a) and diameter (Fig. 5b) distributions for the MVE at condition 22 in Table 1. The volume-weighting effect of particles in the coating also has implications for sensor dynamic range (discussed further

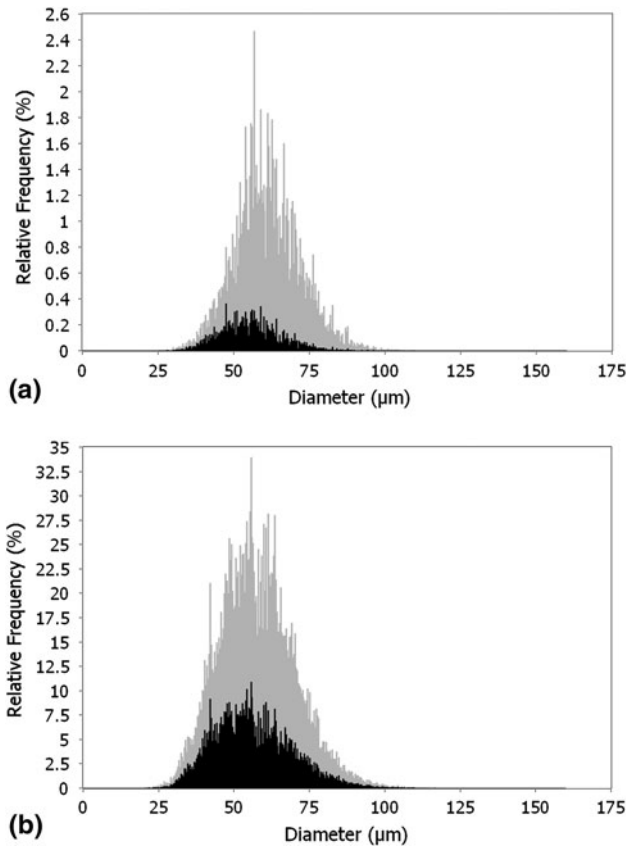


**Fig. 4** Number weighted histogram of diameter showing the differences between the total ensemble (*gray*) and the MVE (*black*) for conditions 4 (a) and 7 (b) in Table 1

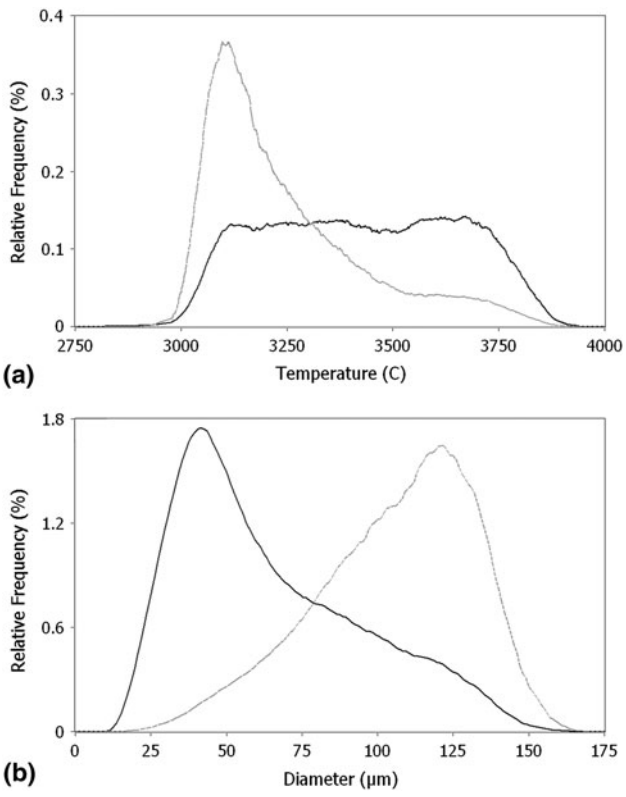


**Fig. 5** Volume (*gray*) and number (*black*) weighted distributions of (a) temperature and (b) diameter of only molten particles (condition 22 in Table 1)

in Section 5). Since most sensors cannot capture the entire ensemble of particles in the plume distributions, the sensor should be targeted toward the particles that contribute the largest volume to the MVE, not just those that contribute the greatest number of particles (i.e., smaller particles).

### 4.2 Spatial and Temporal Distributions

Since the MVE is distributed nonuniformly across the plume, contributions to the coating will be biased to conditions near the region where molten volume flux is highest. This impacts the geometry of the deposition path on the part, but also has implications for sensor measurement volume size and location. The variation in molten volume flux in the vertical distributions (direction of injection) is shown in Fig. 6 along with similar profiles for mean temperature, mean particle light intensity and particle flux (number of particles per second). The centroid of the light intensity distribution is often taken as a marker of the sweet spot of the plume, and as shown in Fig. 6, the peak in the light intensity is close to, but not coincident with, that of the molten volume flux distribution.

The various quantities in Fig. 6 are normalized based on the maximum and minimum of the number-average values for conditions 21-28 in Table 1, measured at the light intensity centroid. For example, for temperature,

$$T^* = \frac{T - T_{\mathrm{MIN}}}{T_{\mathrm{MAX}} - T_{\mathrm{MIN}}}. \qquad \text{(Eq 5)}$$

Using this normalization, the variations in the plume can be viewed in relation to the variations expected when torch conditions are changed. Therefore, for the case shown in Fig. 6, the variation in mean particle temperature across the plume is larger than the variation in mean temperature seen across conditions 21-28 in Table 1, which is an important factor when considering the use of temperature for control purposes (Section 5.3). In particular, these results suggest that it is critical to develop a consistent scheme for determining where the measurement volume should be positioned based on the actual spatial distribution of the critical distribution.

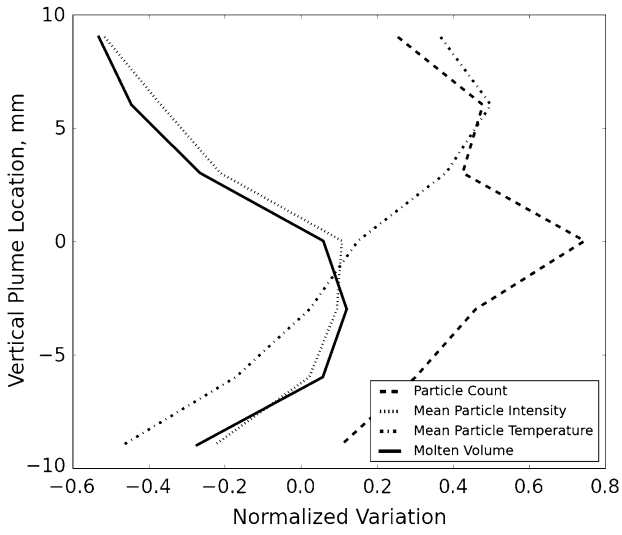


**Fig. 6** Vertical plume profiles from DPV of molten volume flux (*solid*), number-average temperature (*dash-dot*), particle flux (*dashed*), and total light intensity emitted by particles (*dotted*). Normalization method is shown in Eq 5 (condition 28 in Table 1)

In addition, there are significant temporal fluctuations of sensed particle states, as seen in the molten volume flux time series shown in Fig. 7. Filtering through moving ensemble averaging reduces the magnitude of the fluctuations significantly (white line in Fig. 7), and is important to consider in developing an appropriate signal for control purposes. However, the size of the averaging window must be small compared to the time scales of the process that need to be controlled (see Section 6), otherwise the variations that need to be controlled will be lost in the averaging. Uncertainty from under sampling can be more pronounced with volume-weighted conditions, such as the MVF, since they may be biased by a few large particles that appear in a small ensemble. This means that volume-weighted averages may require more particles for proper determination when compared to number-averaged quantities.

## 5. Measurement Issues

### 5.1 Dynamic Range

For sensors that sequentially measure individual particles, one sensing element collects all available light from the particle, regardless of particle size. Since the amount of light emitted by a particle is proportional to the surface area of that particle (and the fourth power of temperature), the intensity of light measured by such a sensing scheme is proportional to $D^2T^4$. For plasma-sprayed YSZ thermal barrier coatings, detected particle temperatures may span a temperature range of 2000-4000 K, for particles that range from 10 to 90 μm in diameter, so the largest particle at the highest temperature will emit light 1296 times more intense than the smallest, coldest particle. Therefore, a conventional sensor must have a dynamic range of 1296 (31 dB) in order to detect and measure all particles taking part in the process. Since this range is beyond the capability of most optical sensors, given typical signal-to-noise ratios, some of the particles in the plume will be undetected.

For a CCD array that images diameter directly, the required dynamic range is reduced, since the light from the particle is spread over several pixels. In addition, the integral nature of the sensed image means that the total intensity of the radiation is proportional to time during which the particle is in the field of view of the sensing element (sensing time), a quantity that is in turn proportional to diameter to the first power. Both of these effects reduce the required dynamic range for CCD array sensors compared to single element sensors; the exact value of this reduction will depend on the size of the sensing elements

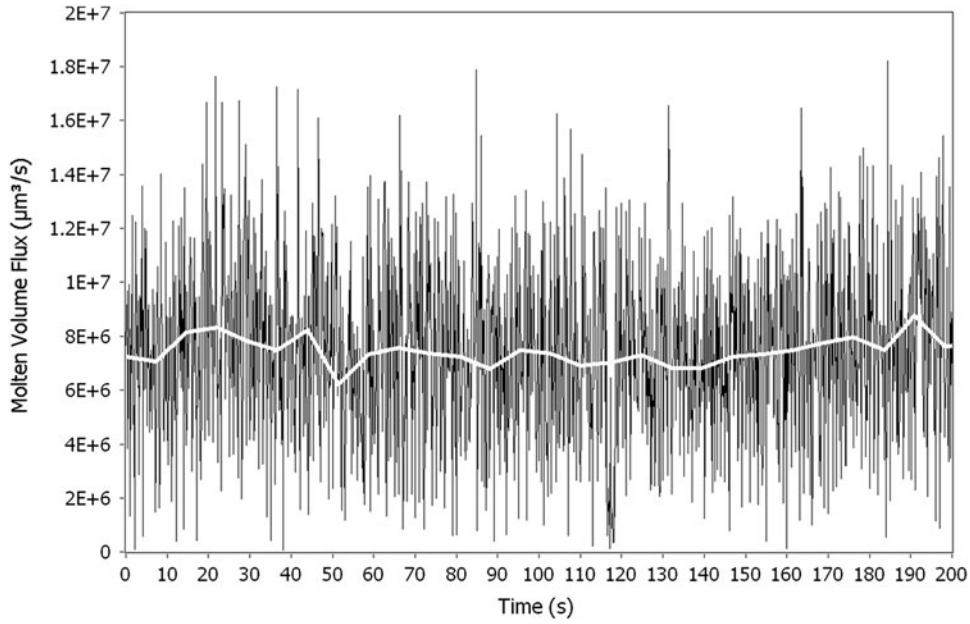


**Fig. 7** Time variation in molten volume flux (*black line*) and a 1000 particle moving average of molten flux (*white line*) (condition 35 in Table 1)

and the range of particle diameters, but it can be as much as a factor of 10. Note that this effect is mitigated by the fact that the sensing time is also proportional to $1/v$ where $v$ is velocity, reducing sensitivity to faster moving particles. Despite the wider dynamic range of CCD arrays, they, like single particle sensors, cannot capture the entire range of particles in the plume. As such, any sensor must be operated in a manner that preferentially captures the critical subdistribution of particles that contribute to the coating. In particular, it should capture medium-sized particles that are small enough to melt but large enough to contribute significant volume to the MVE.

### 5.2 Temperature Measurement

The temperature distribution shown in Fig. 8 features a peak at 3150 °C, followed by a second broader peak around near 3400 °C. This type of bimodal distribution has been observed and analyzed in Ref 7 and 8. In particular, the peak at lower temperatures persists as conditions are changed, suggesting that it represents the melting temperature range (liquidus to solidus). However, this peak does not align with the expected melting temperature of the feed stock material (Ref 7, 8) (in the case shown in Fig. 8, 2678-2753 °C for 8 wt.% YSZ). A possible explanation for the discrepancy is the difference in the emissivity-wavelength relation between the sprayed materials and the tungsten ribbon filament used for calibrating the DPV 2000 (Ref 7), an effect that could lead to measurement errors as large as 20% (Ref 9). In particular, for molybdenum and tungsten, predicted errors based on known emissivity behavior of the powder material, combined with errors due to the breakdown in the assumed linear calibration relation about 3250 °C, were consistent

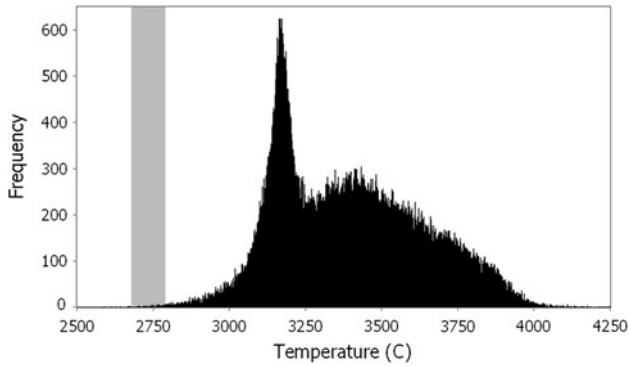


**Fig. 8** Particle temperature distribution, showing a peak that should correspond to melting temperature measured by the DPV. The *gray shaded area* is the melting temperature range for 8 wt.% YSZ (condition 35 in Table 1)

with the offset between the distribution peaks and the melting temperature (Ref 8). If further evidence shows that this peak does represent the melting temperature, then it may provide an in situ method for calibration of two-color systems. In particular, such a calibration could be extremely important for finding molten volume flux, or other metrics of the MVE, since it could provide a definitive boundary between molten and nonmolten particles. In our experiments, however, we consider a particle to be molten if its observed temperature exceeds the known melting point of the material.

The optical depth of ceramic particles such as YSZ is such that larger particles may be opaque (optically thick), smaller particles may be transparent (optically thin) and intermediate particles may be semi-transparent (optical

depth on the same order as the diameter). For the latter two conditions, optical sensors will capture radiation from regions inside the particle. In the presence of temperature gradients, the sensed ''color'' temperature will be some average of the temperatures inside this volumetric radiation zone rather than a measurement of surface temperature. One could argue that such a measurement is more representative of the particle enthalpy state than the surface temperature alone, but the variation of the effect among all particles in the plume may make it hard to interpret data (e.g., understanding various peaks in the temperature distribution, Ref 8). Although radial temperature gradients for YSZ particles can be large near the torch exit, they decrease during the cooling phase as the particle approach the substrate (Ref 10). This might imply that volumetric radiation effects are small at typical sensor locations (Ref 9), though more analysis is needed to determine the effects of particle size and plasma conditions.

### 5.3 Sensor Positioning

For single particle measurement systems, such as the DPV 2000, the measurement volume is much smaller than the dimensions of the plume, so proper sensor positioning is critical. To sense at a single location, the DPV uses an auto-centering algorithm, which is the origin of the axes shown in vertical scans in Fig. 6. As seen in that figure, the position aligns with the peak in number flux, light intensity, and molten volume. However, the temperature gradient is steep near this location, so that small misalignments of the sensor could lead to errors in the measured temperature. Sensors based on CCD arrays can have measurement volumes that span the entire plume, so they can provide plume-wide measurements that eliminate position-based biasing. Full-plume scans can be generated using small measurement-volume sensors as well, but the time needed to scan the full plume may be prohibitive for control purposes (Section 6).

### 5.4 Diameter Measurement

Though accurate diameter measurements are not important when developing a sensor signal based on bulk or particle averaged values, it is critical when using volume-weighted quantities like molten volume flux since volume is proportional to the diameter cubed. With single element sensors, diameter is determined through the relation among peak light intensity, diameter, and temperature (Eq 1). This approach has several issues. First, any errors in temperature (Section 5.2) or light intensity measurements will propagate through the calculation of diameter, increasing the uncertainty in that value. Second, if the constant of proportionality, a function of sensor properties and emissivity of the particles, cannot be determined a priori, then it must be found through calibration. A typical approach is to match the peak of the measured diameter distribution to that of the powder feedstock; however, the diameter of a plasma densified powder particle is expected to change upon complete melting. Furthermore, the sensor-measured diameter distribution is distorted due to the limited dynamic range. This approach can provide an order of magnitude calibration useful for qualitative trends, but one that may not be accurate enough for volume-weighted analysis (See discussion of Fig. 13 in Section 6). Finally, the volumetric radiation effect, described in Section 4.2, will lead to additional errors, not only because of errors in temperature, but also because the radiated light intensity will no longer follow a simple functional relation with diameter. Opaque particles will follow a $D^2$ trend, transparent particles would follow a $D^3$ trend and semi-transparent particles would likely follow a trend between $D^2$ and $D^3$.

CCD arrays that directly measure diameter do not require calibration, and therefore have an advantage for molten flux sensing and control. However, the smallest particle that can be sensed is limited by the size of pixels in the array and the noise in the signal. This is mitigated by the fact that smaller particles contribute less volume to the deposited coating, but must be considered nonetheless.

### 5.5 Biasing of Bulk Ensemble Averages

Measurements by sensors that provide bulk averages of temperature via pyrometry of light collected over a large area and integrated over a long time are biased by large, hot particles since the light intensity of any given particle is proportional to $D^2T^4$. The errors in temperature measurement associated with these biases have been analyzed in (Ref 9) for YSZ with predicted errors on the order of 10% or less for mean particle temperatures greater than 2500 K.

There is also a velocity bias in bulk measurements, since the collected radiation is proportional to the particle residence time or $1/V$, so that more radiation is collected from slower particles. This was noted for the correlation coefficient approach used for ensemble velocity measurements by the Accuraspray (Ref 11). For temperature, it was conjectured that this effect would be obscured by the fact that fewer slower particles arrive in a measurement volume (Ref 9), thus weighting particles the same regardless of velocity. However, if fewer particles arrive at the substrate at any given time, then they should actually be weighted less than, not the same as, faster moving particles that arrive more often. Thus, the velocity bias of bulk temperature measurements should be a concern.

## 6. Experimental Sensor Evaluation for Deposition Rate Control

Sensors can be used in plasma spray for a variety of purposes:

(a) as a tool to reduce production variation for a specific booth, either through manual or automatic control to compensate for process variations, as well as to maintain optimized deposition conditions,

(b) as a tool to aid in developing process conditions for new applications, new powders, or new guns, and
(c) as a tool to maintain consistency from booth-to-booth and plant-to-plant.

It is important to match the attributes of the measurement to the application. Specifically, it is important to relate a sensed quantity to some specification of the coating that represents the objective of a particular application. The focus in this section is to examine measurement schemes that can be used for maintaining a desired deposition rate. Beyond deposition rate control, it is important to be able to optimize deposition conditions to minimize cost (such as finding the injection conditions that maximize deposition efficiency), as well as to control the quality and properties of the coating structure, but will be reported in future studies.

### 6.1 Experiments

To develop an understanding of which sensing strategies and measured values best correlate to the deposited mass, experiments were conducted using a internal (SG 100) and external (F4 and 9 MB) injection torches. The torch operating conditions are listed in Table 1, and had deposition rates roughly on the order of 20 μm thickness per pass. The input conditions (torch current, flow rate, and carrier gas flow rate) were varied to examine a broad range of deposition rates, in order to examine a range of conditions to evaluate how well the measured plume particle states correlate to the deposited mass. While changing the flow rate does not directly correspond to open-loop torch variation, it is relevant in terms of the result of active control as well as exploring alternative operating conditions. Reports on experiments designed to mimic torch aging/variation will be the subject of future work.

Two sensor systems were used to obtain data: the DPV and the Flux Sentinel. These two systems were used because they obtain individual particle data that can be used to determine molten mass flux for both a single location as well as across the whole plume. They differ, however, in the measurement engine used, and thus have different sensitivities to particle characteristics (temperature, velocity, and diameter). From the individual particle data, estimates can be made of plume and bulk-average measurements, such as would be obtained by other sensing schemes. A major difference between the two sensors is that the DPV obtains data in a small measurement volume and relies on a translation system to obtain a plume scan, while the Flux Sentinel captures data from the entire plume height without translation. Important issues addressed by the experiments include: correlation of the sensing strategy to deposited mass, the number of particles that need to be measured to provide a robust signal characteristic of the particle ensemble average, and the sensitivity of the measurement location.

### 6.2 SG-100 Results

Only the Flux Sentinel was used in the experiments with the SG-100 internal injection torch. Correlations between deposited mass and whole plume averaged temperature, average temperature at the centroid, plume light intensity, and molten mass flux are shown in Fig. 9. These correlations were obtained for perturbations in torch current and flow rate as well as carrier gas flow rate. One metric of how well a linear regression can fit this data is the square of the sample correlation coefficient, or $R^2$, which varies between 0 and 1, 1 indicating perfect correlation and 0 indicating no correlation between the two variables. From these experiments, both molten flux ($R^2 = 0.92$) and light intensity ($R^2 = 0.86$) correlate well to the deposited mass. Neither the whole plume ($R^2 = 0.67$) nor the centroid temperatures ($R^2 = 0.03$) correlated as well as molten volume flux. However, in other experiments conducted using the SG 100, light intensity does not always correlate well as shown in Fig. 10 (Ref 5).

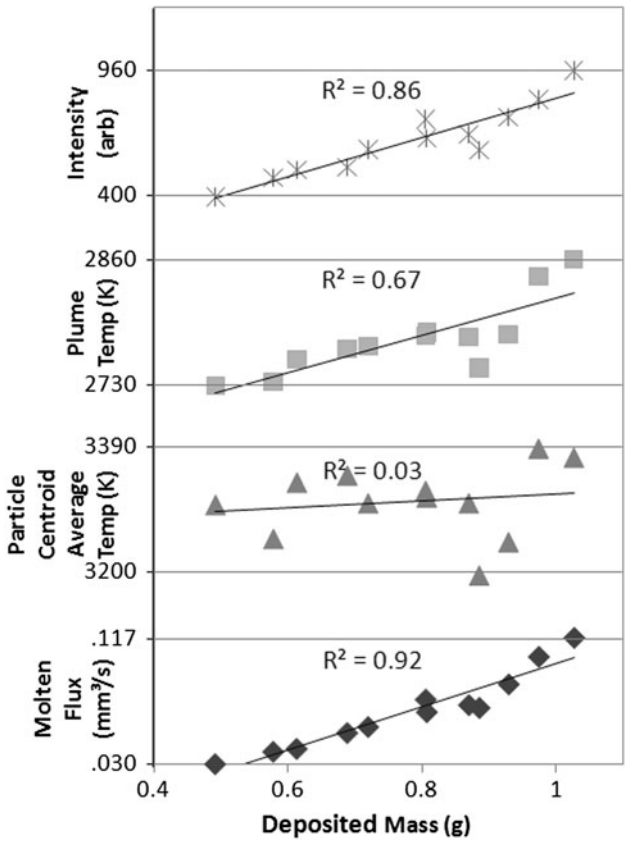


**Fig. 9** Correlations between deposited mass and plume light intensity (*asterisks*), whole plume temperature (*squares*), average particle temperature at the centroid (*triangles*), and molten mass flux (*diamonds*) for a SG100 torch measured with the Flux Sentinel (conditions 8-19 in Table 1)

In comparing temperature measurements from the whole plume to those taken at the centroid, it is observed that the range of temperature change is smaller for the whole plume temperature measurement than for the centroid measurement. The reason is that the whole plume measurement is an average from all the observed particles in the plume and thus corresponds to a broader distribution of particle states. This effectively reduces the

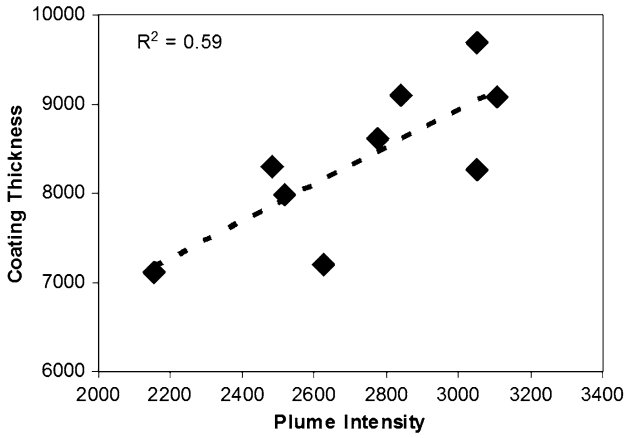


**Fig. 10** Correlation between plume light intensity and coating thickness (Ref 5)

sensitivity of the measured temperature to changes in any one part of the particle distribution. In general, measurements made at the centroid are subject to errors in locating the centroid position from one measurement to another, and one must make an additional decision as to which centroid to locate. As seen in Section 5.3, for some operating conditions, the centroids of molten flux, temperature, and light intensity do not necessarily all coincide. Thus, measuring the molten flux at a location selected by any one of those might not yield consistent results and good correlations with the deposited mass. Additionally, results show that number flux might not be well correlated to molten flux since it could tend to weight the large number of smaller particles to a greater extent and it includes nonmolten particles. Thus it may not be a suitable metric to determine the centroid position.

### 6.3 9 MB and F4 Results

Results for external injected torches are more variable. In some cases, good correlations were obtained, while in seemingly similar cases the correlations were quite poor. Two results obtained for a 9 MB gun suggest that the issue might be due to the interaction of sensor limitations with changes in the distribution of the particle ensemble that occur as the centroid shifts. In particular, a shift of the centroid in space implies that the particles are following different trajectories in relation to the plasma plume, and must result in a different distribution of particle states. Thus, since it is likely that the sensor is only able to image a subset of the entire particle ensemble, a large shift of centroid position might also change the measured subset of particles, and thus result in a poor correlation. Figure 11 shows good correlation of molten flux to deposited mass for the 9 MB where only current is changed. This experiment was conducted based on previous experimental results (Ref 12) that have shown that changes in torch current have a minimal impact on centroid location, somewhere on the order of 1 mm. In contrast, when perturbations entail a large change of centroid

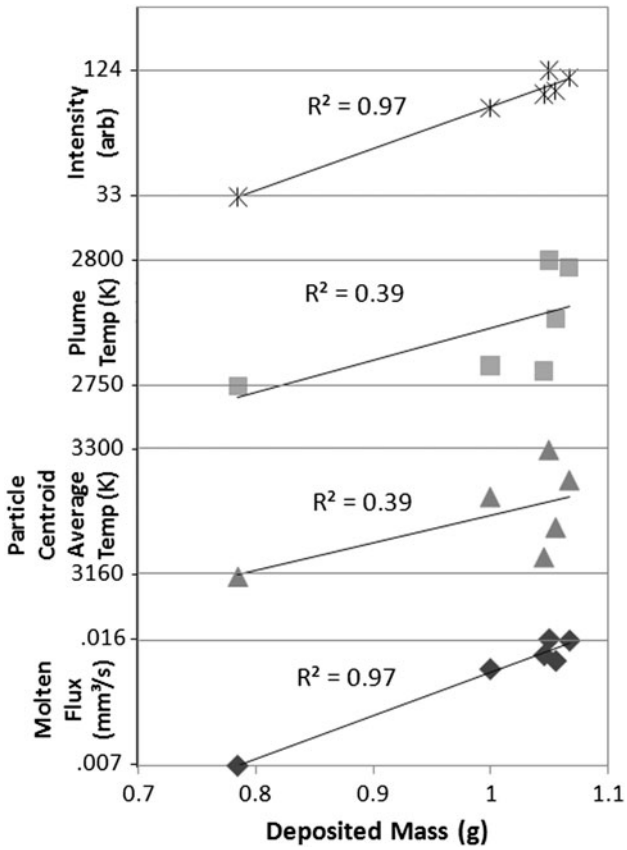


**Fig. 11** Correlations between deposited mass and plume light intensity (*asterisks*), whole plume temperature (*squares*), average particle temperature at the centroid (*triangles*), and molten mass flux (*diamonds*) for a 9 MB torch measured with the Flux Sentinel (conditions 29-34 in Table 1)

position (4.06 mm spread between conditions 21-28 in Table 1), the correlation is poor not only for plume light intensity ($R^2 = 0.44$), plume temperature ($R^2 = 0.28$), and average particle temperature at the centroid ($R^2 = 0.11$), but also for molten volume flux ($R^2 = 0.54$, Fig. 12). These results are consistent with suggestions to maintain a constant centroid position while making measurements by adjusting the carrier gas flow rate (Ref 13). As suggested by Srinivasan et al., this is done to "maintain comparable plume trajectory for the different process conditions," as well as to operate under injection conditions that optimize the particle distribution temperature and velocity (Ref 13).

A series of perturbation experiments were conducted with an F4 torch, using both the DPV and Flux Sentinel, but adjusting carrier gas input to maintain the molten flux centroid within 1 mm from condition to condition. In this way, a very high correlation was attained, as shown in Fig. 13, even though the F4 uses external injection. Correlations with centroid and whole plume temperature were markedly worse (Fig. 14). While more experiments and analysis must be conducted to confirm these results, it appears that centroid control is not only important for

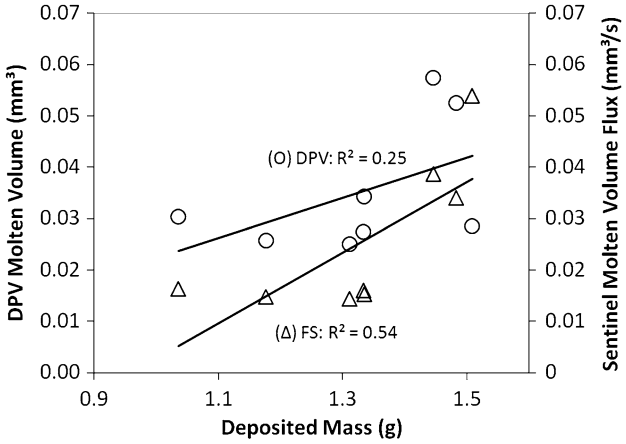


**Fig. 12** Correlation of molten volume flux from both the DPV-2000 (O's, $R^2 = 0.25$) and Flux Sentinel (Δ's, $R^2 = 0.54$) sensors to deposited mass for torch input perturbations in torch gas flow rate, carrier gas flow rate, and torch current using a 9 MB torch (conditions 20-28 in Table 1)

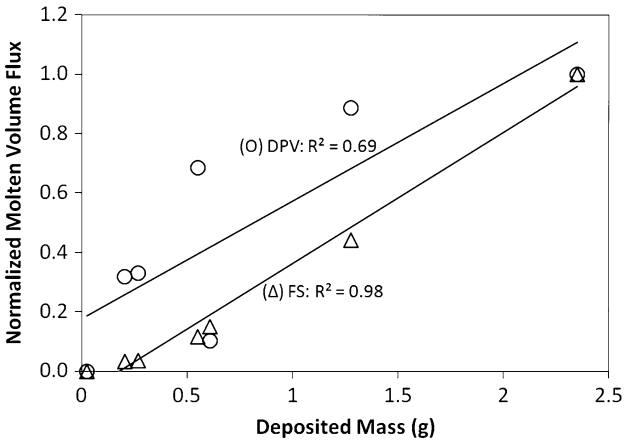


**Fig. 13** Correlation of molten volume flux from both the DPV-2000 (O's, $R^2 = 0.69$) and Flux Sentinel (Δ's, $R^2 = 0.98$) sensors to deposited mass for torch input perturbations in torch gas flow rate, secondary gas percentage, and torch current using a F4 torch. Manual molten centroid control was performed using carrier gas adjustments and Flux Sentinel output (conditions 1-7 in Table 1)

maintaining the desired spray location, but also for consistent measurements.

In interpreting these experimental results, it is important to recognize that deposition conditions, such as variations in substrate temperature as well as fixturing, could have introduced variations. Specifically, for the experiments described here, the peak substrate temperature varied between 550 and 750 °C, and the substrates were not preheated. Thus, the poor correlation seen in some cases may have been due to variations in deposition conditions at the substrate because of their different temperatures. However, for some experiments, good correlation was achieved even though the measured

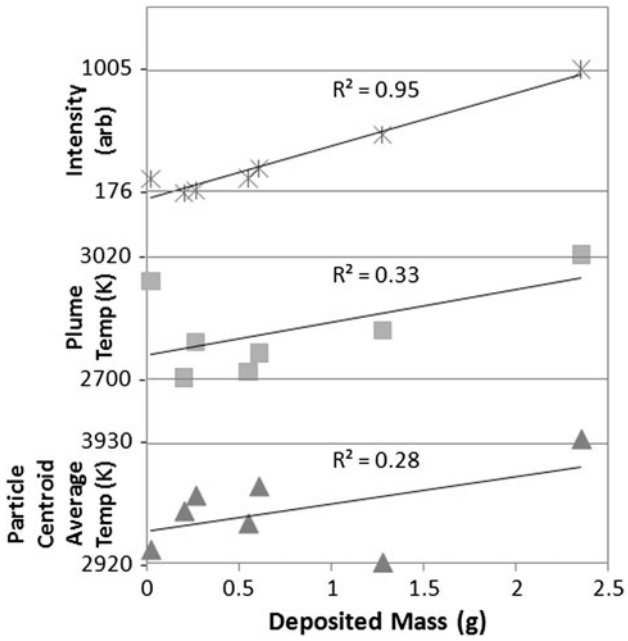


**Fig. 14** Correlations between deposited mass and plume light intensity (*asterisks*), whole plume temperature (*squares*), and average particle temperature at the centroid (*triangles*), a using an F4 torch measured with the Flux Sentinel. Manual molten centroid control was performed using carrier gas adjustments and Flux Sentinel output (conditions 1-7 in Table 1)

substrate temperature varied by hundreds of degrees (Fig. 11). This issue will be addressed in a future paper once a substrate temperature control procedure has been implemented.

Whether using a DPV or a Flux Sentinel, it is important to consider how many data points are needed to establish a tight correlation between the sampled ensemble and the ensemble average, particularly if control action is going to be based on the measurement. Using the DPV with the 9 MB torch, particle state data were collected for 100,000 particles at the point obtained from the DPV's centering algorithm for condition 35 shown in Table 1. Different sample sizes between 100 and 25,000 were selected, and the standard deviation of each subsamples plotted in Fig. 15. A different normalization procedure was used for each of the variables to reflect their specific ranges: temperature was normalized by 200 °C since this is on the order of magnitude of the change of temperature for the experiments conducted in this study, while molten flux was normalized by the average molten flux number. The plot shows that both variables are sufficiently sampled by 5000-7000 particles.

## 7. Implications for Control Sensor Requirements

The experimental results reveal that there are a variety of factors that should be considered in selecting a sensing

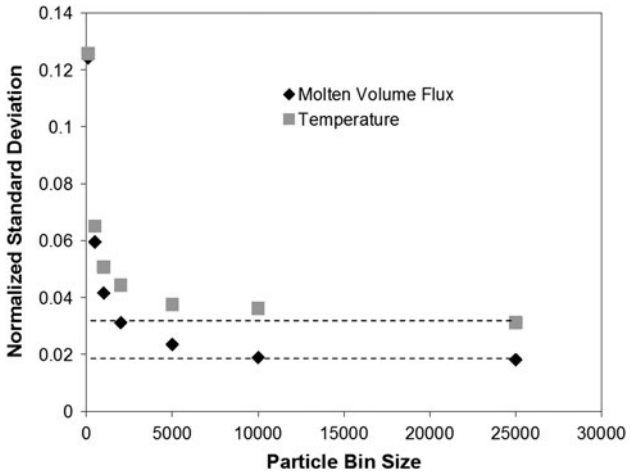


**Fig. 15** Normalized standard deviation of temperature (*gray squares*) and molten volume flux (*black diamonds*) from subsamples of data obtained with the DPV-2000. The molten volume flux was normalized by dividing each standard deviation by the average molten volume flux, while the temperature was normalized by dividing each standard deviation by 200. The temperature was divided by 200 in order to match the range of temperatures observed (condition 35 in Table 1)

approach that is sensitive to deposition rate and is useful both for implementing real-time control as well as for providing information for operator-based adjustment.

(a) The sensor should be able to measure mass flux since this avoids any bias due to a large number of smaller particles. However, mass (or volume) flux is determined indirectly through measurement of the particle diameter, which is converted to volume, and the particle flux rate. Therefore, the sensor must provide accurate diameter measurements, which could pose a problem for those sensors that rely on an indirect method based on the relationship among diameter, measured light intensity, and temperature and require a calibration constant that is difficult to determine accurately.

(b) The sensor should detect the molten particle characteristics: effective control of coating thickness requires the ability to regulate the mass flux of molten particles, which dictates the need to measure individual particle temperature, not just an ensemble average. As seen in Fig. 4(a) and (b), the diameter distribution of the molten particles is significantly different from that of the nonmolten particles, and thus control of overall ensemble averages would be skewed toward larger mostly nonmolten particles that are not incorporated in the coating.

Points (a) and (b) highlight the need for individual particle measurement schemes instead of bulk averages since a conditioned averaged of mass or volume flux (requiring knowledge of particle diameter) and screening based on particle temperature is required.

(c) The sensor should image the whole plume at a rate commensurate with the control needs of plasma spray processes: Small-area (diameter ~1 mm) single-point measurements of particle characteristics and the variation of these characteristics with torch input changes can be sensitive to the location selected. Thus, a parameter obtained by a whole plume (~20 mm) is more robust to changes in plume location. However, to gather enough data to obtain a well-conditioned measurement value (on the order of 5-10,000 particles) at the required location if not for the whole plume, an effective sensor for real-time control should provide full-plume measurements at a rate of 0.1 Hz, This implies requiring measurement rates of around 500-1000 particles per second.

(d) If a sensor with a small measurement volume relative to the plume is used, then the sensor should also be able to quickly determine the spatial distribution of particle characteristics in order to ensure that the centroid position can be measured for control. As shown by some experiments, different operating conditions result in different spatial distributions of particle/plume attributes (e.g., light intensity, particle flux, and temperature). Thus, statistics across the whole plume must be obtained in timely fashion to determine the location of the desired centroid. This can then be used as the basis for implementing automatic centroid position control of the appropriate variable (e.g., light intensity, molten flux, or temperature), which is important not only for maintaining uniform spray location relative to the part, but also for obtaining a consistent particle ensemble for the sensors observation capabilities.

(e) The sensed parameter should exhibit large sensitivity to changes in torch conditions, also have good correlation to the control variable. If the correlation is poor, then the controller will act to change the inputs in cases where it is not warranted.

## 8. Conclusions

This paper discussed the requirements of sensors for deposition rate control for plasma spraying of thermal barrier coatings. Experiments with different torches showed that molten volume flux measured across the entire plume correlated better with deposited mass than other quantities: number-average particle temperature at the centroid, plume bulk temperature, and overall plume light intensity. The best correlations were achieved when the location of plume centroid was approximately constant, highlighting the importance of centroid position control.

Implementing control of molten volume flux combined with centroid control places more stringent demands on required sensor capabilities than those required for control of average particle temperature or velocity alone. These include: the ability to selectively sense individual

particles in the MVE; the ability to accurately measure diameter in order to ensure the proper volume-weighted contributions of individual particles to the molten volume flux; the ability to sense the entire plume and capture a large enough ensemble of particles at a rate commensurate with the demands of real-time control (about 1000 particles per second); and the ability to quickly determine the plume centroid. Various sensor schemes were reviewed within the context of these requirements, and it was shown that CCD arrays provide important advantages in meeting the requirements of molten volume flux control. A new CCD-based sensor has been developed for this purpose, and experimental correlations with deposited mass have been promising.

## Acknowledgments

This material is based in part upon work supported by the National Science Foundation under Grant Numbers DMI-0300484, OII-0539622, and IIP-0724382. The authors gratefully acknowledge the contributions from undergraduate students who aided in conducting experiments and analyzing the results including Sean DeLeo, Annie Lum, Steve Maouyo, and Kristina Hogstrom.

## References

1. M.A. Khan, C. Allemand, and T.W. Eagar, Non-Contact Temperature Measurement for Process Diagnostics, *Proc. Materials Research Society Symposium on process Diagnostics: Materials, Combustion, Fusion*, Materials Research Society, 1988, p 117-119
2. C. Moreau, P. Gougeon, M. Lamontagne, V. Lacasse, G. Vaudreuil, and P. Cielo, On-Line Control of the Plasma Spraying Process by Monitoring the Temperature, Velocity and Trajectory of In-Flight Particles, *Thermal Spray Industrial Applications*, C.C. Berndt and S. Sampath, Ed., ASM International, Materials Park, OH, 1994, p 431-438
3. J.F. Bisson, M. Lamontegne, C. Moreau, L. Pouliet, J. Blain, and F. Nadeau, Ensemble In-Flight Particle Diagnostics Under Thermal Spray Conditions, *Thermal Spray 2001: New Surfaces for a New Millennium*, C. Berndt, K.A. Khor, and E.F. Lugsheider, Ed., ASM International, Singapore, 2001, p 705-714
4. J. Vattulainen, E. Hämäläinen, R. Hernberg, P. Vuoristo, and T. Mäntylä, Novel Method for In-Flight Particle Temperature and Velocity Measurements in Plasma Spraying Using a Single CCD Camera, *J. Therm. Spray Technol.*, 2001, **10**, p 94-104
5. B.L. Vattiat, ''Analysis of the Sensor and Measurement Requirements for Feedback Control of Plasma Spray Processes,'' MS Theses, College of Engineering, Boston University, 2004
6. O. Ghosh, ''Modeling and Sensing Strategies of Plasma Spray Particle Distributions for Deposition Rate Control,'' MS Theses, Boston University, College of Engineering, 2007
7. G. Mauer, R. Vaβen, and D. Stöver, Detection of Melting Temperatures and Sources of Errors Using Two-Color Pyrometry During In-Flight Measurements of Atmospheric Plasma-Sprayed Particles, *Int. J. Thermophys.*, 2008, **29**, p 764-786
8. T. Streibl, A. Vaidya, M. Friis, V. Srinivasan, and S. Sampath, A Critical Assessment of Particle Temperature Distributions During Plasma Spraying: Experimental Results for YSZ, *Plasma. Chem. Plasma Process.*, 2006, **26**, p 73-102
9. J.R. Fincke, D.C. Haggard, and W.D. Swank, Particle Temperature Measurement in the Thermal Spray Process, *J. Therm. Spray Technol.*, 2001, **10**, p 255-266
10. L. Dombrovsky, A Modified Differential Approximation for Thermal Radiation of Semitransparent Nonisothermal Particles: Application to Optical Diagnostics of Plasma Spraying, *J. Quant. Spectrosc. Radiat. Transf.*, 2002, **73**, p 433-441
11. G. Bourque, M. Lamontegne, and C. Moreau, Thermal Spray: A New Sensor for On-Line Monitoring the Temperature and Velocity of Thermal Spray Particles, *Thermal Spray: Surface Engineering vi Applied Research*, C.C. Berndt, Ed., May 8-11, 2000 (Montréal, Québec, Canada), ASM International, 2000, p 45-50
12. M. Gevelber, C. Cui, B. Vattiat, D. Wroblewski, J.R. Fincke, and W.D. Swank, Thermal Spray 2003: Real-Time Control for Plasma Spray: Production Issues and Distribution Implications, *Thermal Spray 2003: Advancing the Science and Applying the Technology*, B.R. Marple and C. Moreau, Ed., May 5-8, 2003 (Orlando, FL), ASM International, 2003, p 1121-1130
13. V. Srinivasan, A. Vaidya, T. Streibl, M. Friis, and S. Sampath, On the Reproducibility of Air Plasma Spray Process and Control of Particle State, *J. Therm. Spray Technol.*, 2006, **15**, p 739-743
14. M. Gevelber, D. Wroblewski, B. Vattiat, O. Ghosh, M. VanHout, and S.N. Basu, Issues and Requirements for Developing a Plasma Spray Deposition Rate Sensor for Real-time Control, Thermal Spray, *Crossing Borders*, B.R. Marple, M.M. Hyland, Y.-C. Lau, R.S. Lima, G. Montavon, Ed., ASM International, Maasstrict, The Netherlands, 2008, p 912-916